Electronic Supplementary Material (ESI) for Nanoscale.

SUPPLEMENTARY INFORMATION

Yolk-shell-structured microspheres composed of N-doped-carbon-coated $NiMoO_4$ hollow nanospheres as superior performance anode material for lithium-ion batteries

Gi Dae Park[a], Jeong Hoo Hong[a], Jung-Kul Lee*[b] and Yun Chan Kang*[a]

[a]*Department of Materials Science and Engineering, Korea University, Anam-Dong, Seongbuk-Gu, Seoul 136-713, Republic of Korea, E-mail: yckang@korea.ac.kr; Fax: (+82) 2-928-3584*

[b]*Department of Chemical Engineering, Konkuk University, Hwayang-dong, Gwangjin-gu, Seoul 143-701, Republic of Korea, E-mail: jkrhee@konkuk.ac.kr*

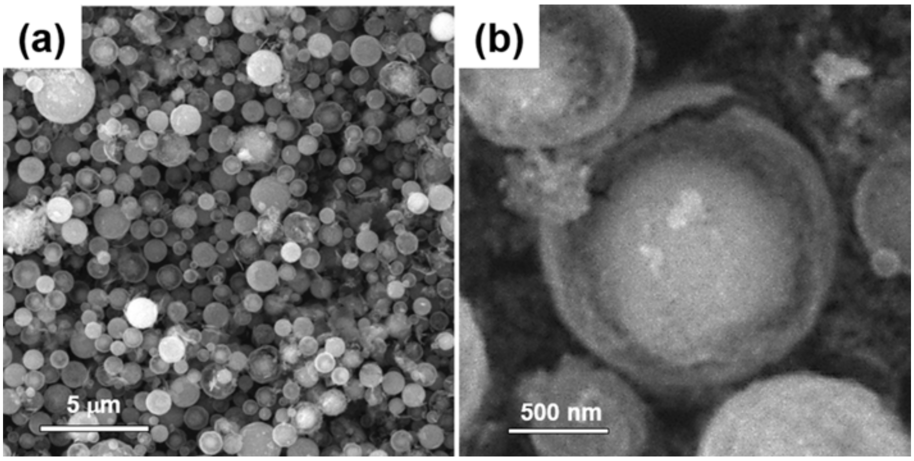

Fig. S1 Morphologies of yolk-shell-structured $NiMoO_4$ precursor microspheres prepared by one-pot spray pyrolysis process.

.

.

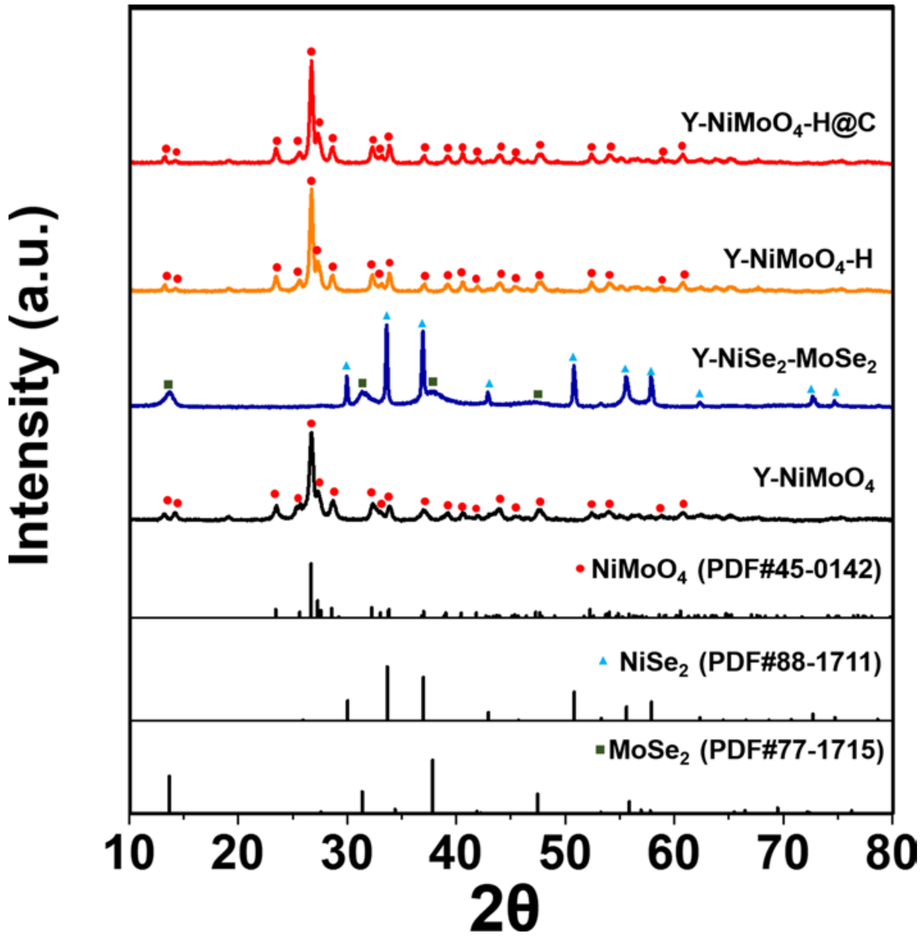

Fig. S2 XRD patterns of yolk-shell-strucutred $NiMoO_4$ precursor microspheres (Y-$NiMoO_4$), Y-$NiSe_2$-$MoSe_2$ composite via the selenization process of Y-$NiMoO_4$, Y-$NiMoO_4$-H via the oxidation of Y-$NiSe_2$-$MoSe_2$, and Y-$NiMoO_4$-H@C via carbon coating process of Y-$NiMoO_4$-H.

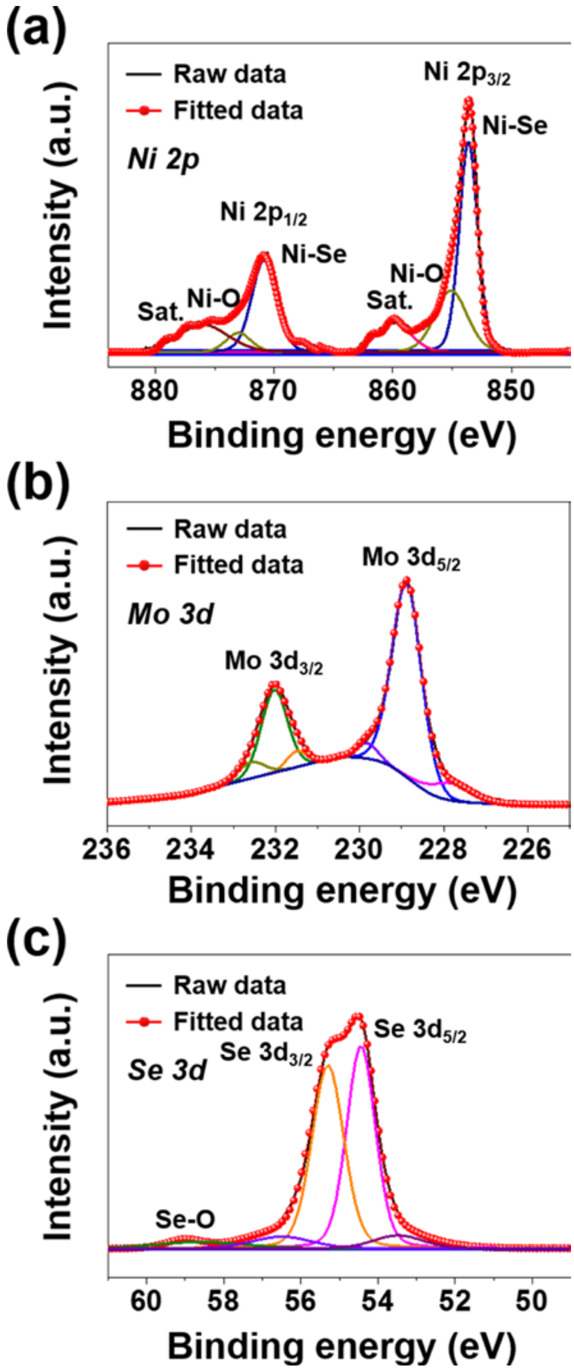

Fig. S3 XPS spectra of yolk-shell-structured $NiSe_2$-$MoSe_2$ composite microsphere: (a) Ni 2p, (b) Mo 3d, and (c) Se 3d.

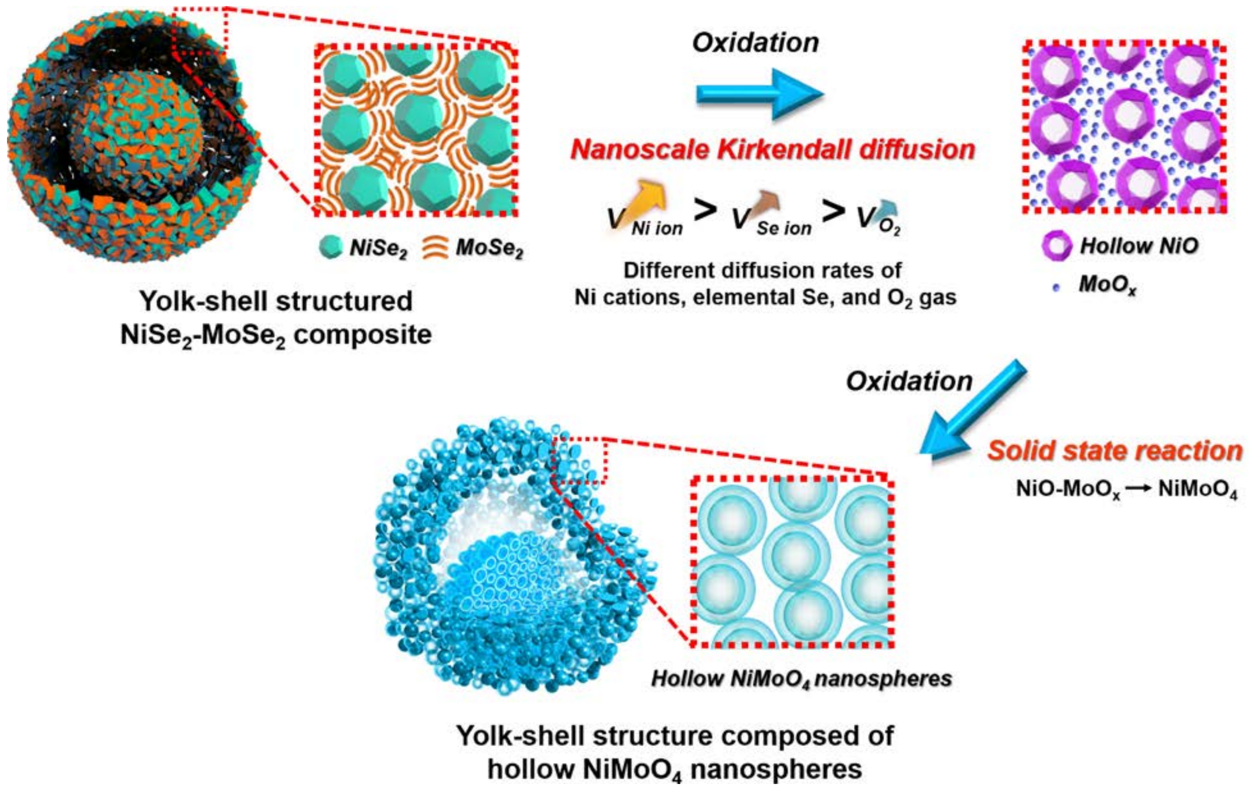

Fig. S4 Formation mechanism of the hollow $NiMoO_4$ nanospheres from $NiSe_2$-$MoSe_2$ composite via nanoscale Kirkendall diffusion.

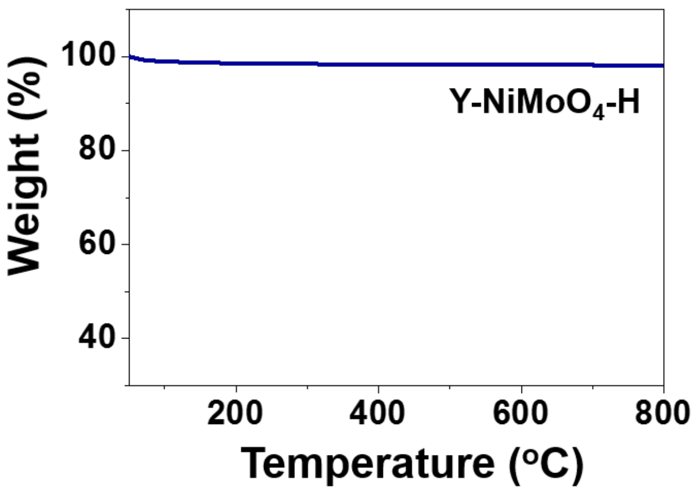

Fig. S5 TG curve of Y-$NiMoO_4$-H measured under an air atmosphere.

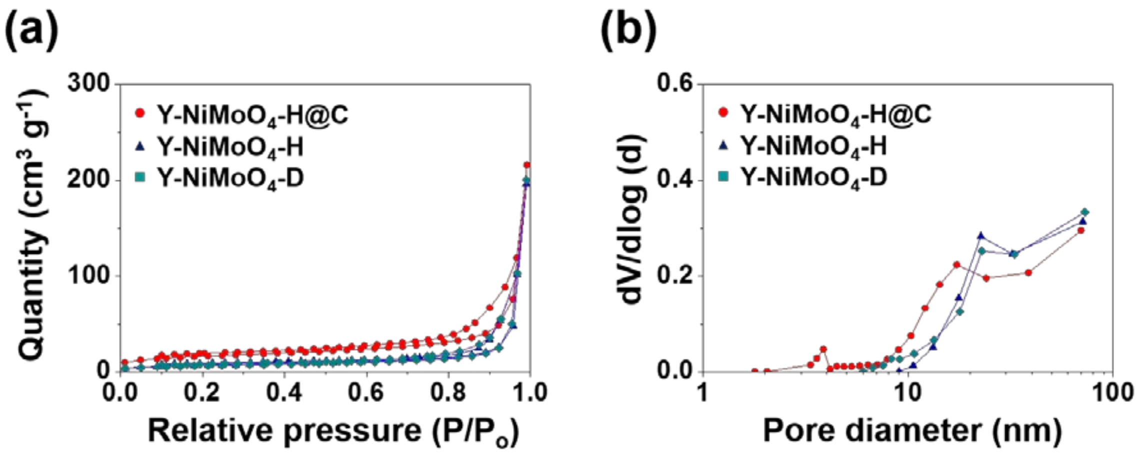

Fig. S6 (a) N_2 gas adsorption and desorption isotherms, and (b) Barrett–Joyner–Halenda (BJH) pore-size distributions of Y-$NiMoO_4$-H@C, Y-$NiMoO_4$-H, and Y-$NiMoO_4$-D.

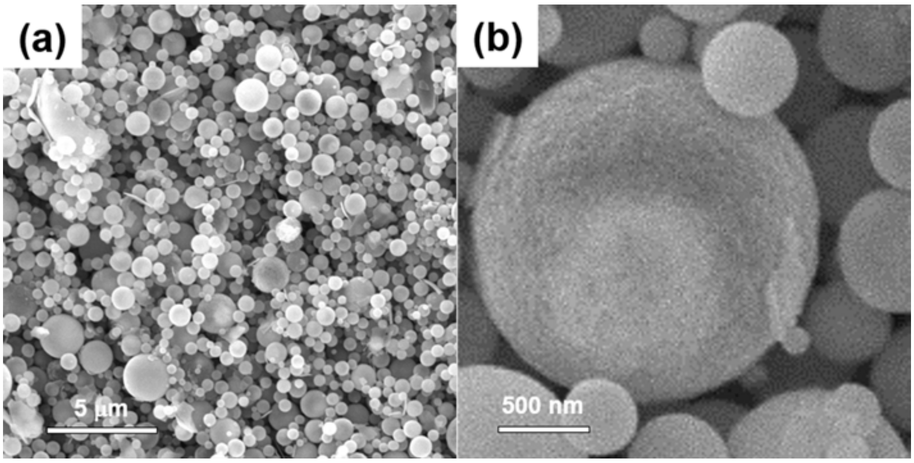

Fig. S7 Morphologies of yolk-shell-structured NiO microspheres prepared by one-pot spray pyrolysis process.

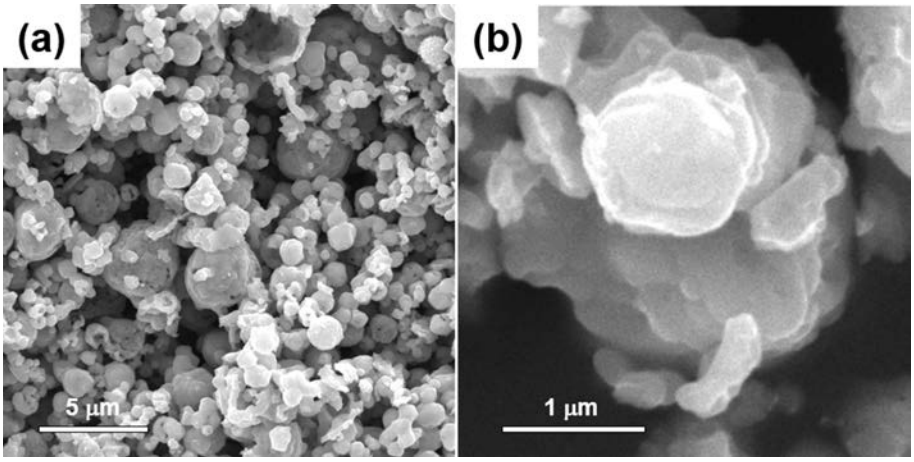

Fig. S8 Morphologies of $NiSe_2$ microspheres prepared by spray pyrolysis and subsequent selenization process.

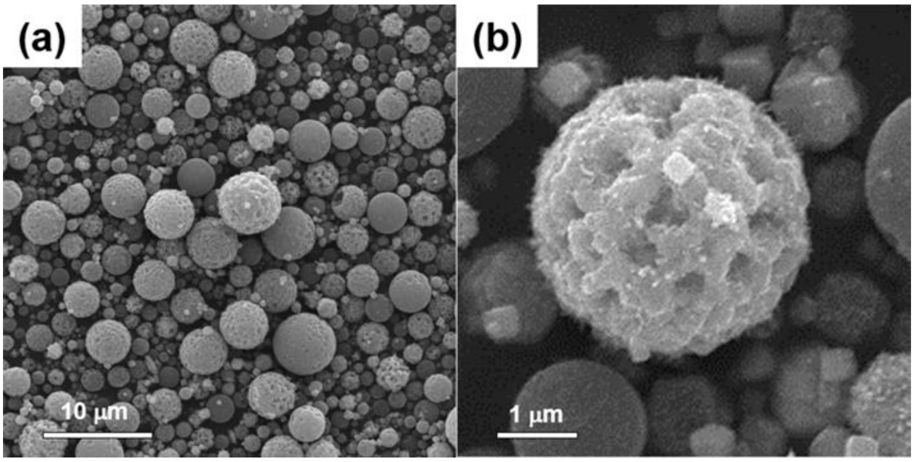

Fig. S9 Morphologies of MoO_3 microspheres prepared by one-pot spray pyrolysis process.

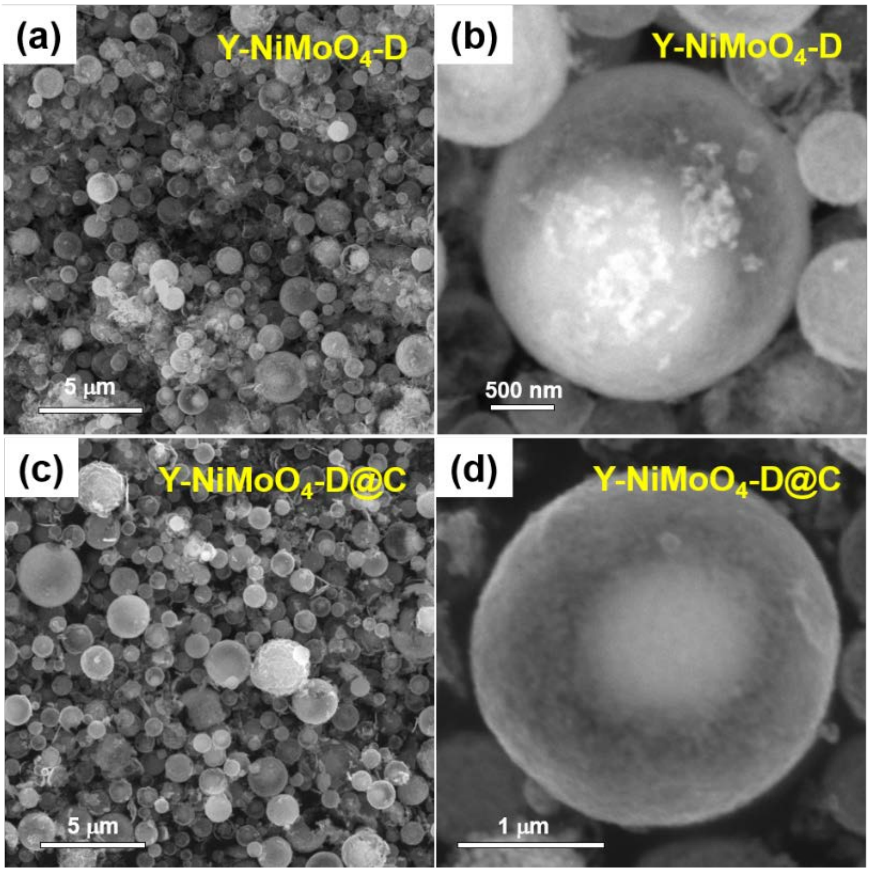

Fig. S10 Morphologies of (a,b) Y-$NiMoO_4$-D and (c,d) Y-$NiMoO_4$-D@C microspheres composed of $NiMoO_4$ dense nanocrystals.

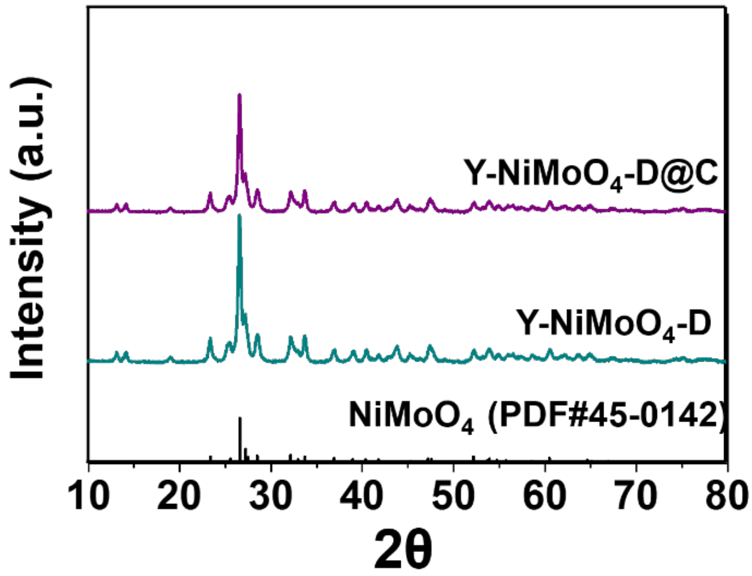

Fig. S11 XRD patterns of Y-$NiMoO_4$-D@C and Y-$NiMoO_4$-D microspheres.

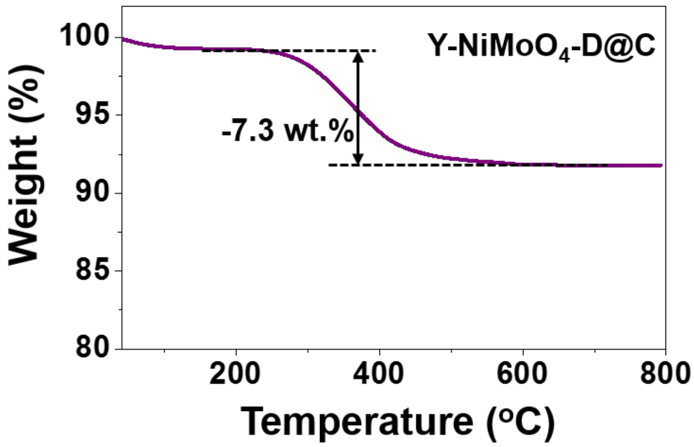

Fig. S12 TG curve of Y-$NiMoO_4$-D@C microspheres.

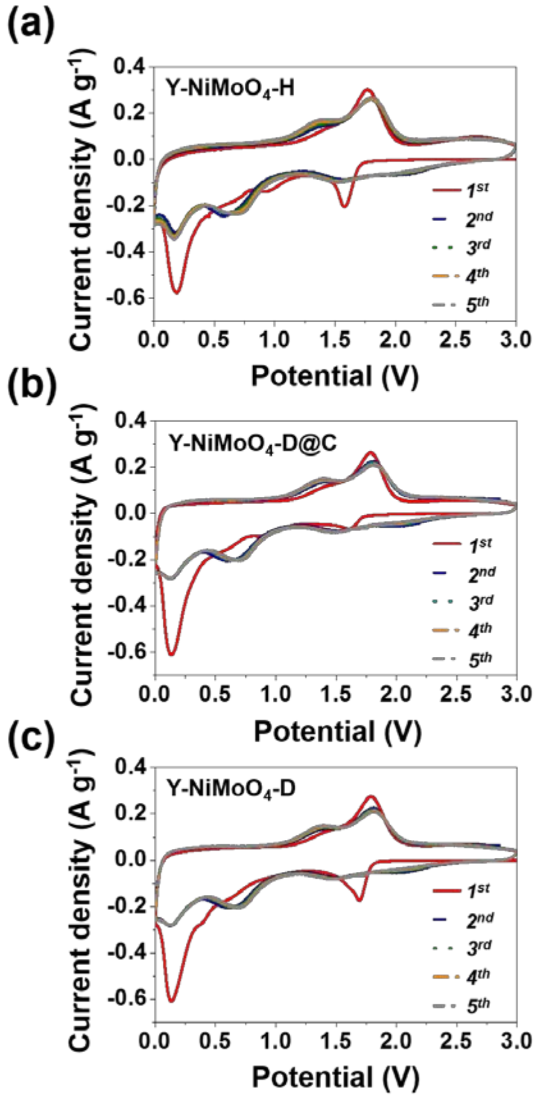

Fig. S13 CV curves of (a) Y-$NiMoO_4$-H, (b) Y-$NiMoO_4$-D@C, and (c) Y-$NiMoO_4$-D.

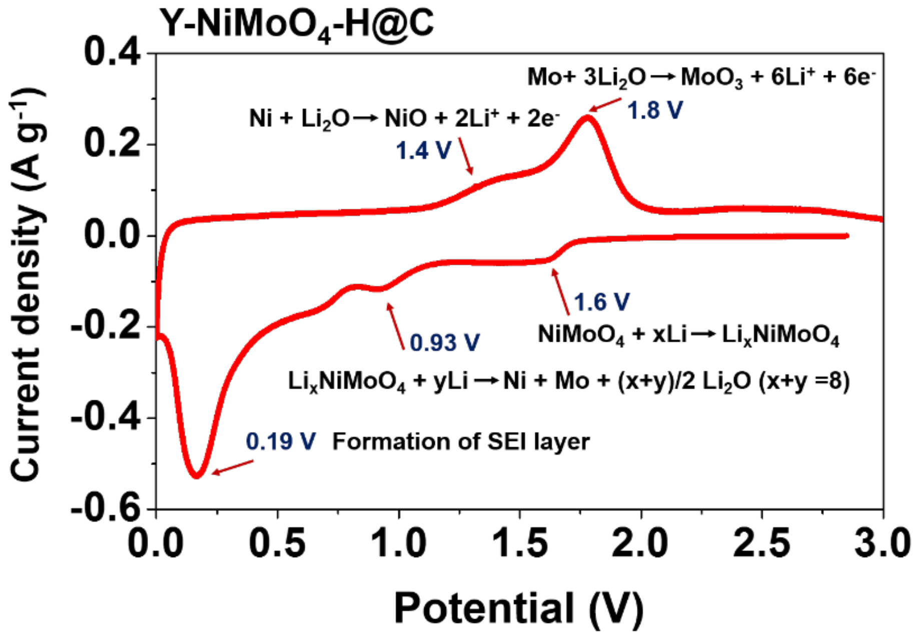

Fig. S14 Redox peaks and the corresponding reactions of yolk-shell-structured $NiMoO_4$ microspheres.

Table S1. Rate performances of various nanostructured $NiMoO_4$ materials with and without carbon material that were reported in previous literature as anode materials for lithium-ion batteries.

Various $NiMoO_4$ materials	Synthesis	Electrochemical properties	Ref
Honeycomb-like $NiMoO_4$ ultrathin nanosheet arrays	Electrochemical method	The discharge capacities were 870 and 370 mA h g^{-1} at current densities of 0.2 and 8.0 A g^{-1}, respectively.	[S1]
Porous $NiMoO_4$ nanoarchitectures on 3D graphene foam	Chemical vapor deposition (CVD)	The discharge capacities were ~1100 and ~600 mA h g^{-1} at current densities of 0.2 and 3.2 A g^{-1}, respectively.	[S2]
$NiMoO_4$ microspheres with numerous empty nanovoids	Spray pyrolysis	The discharge capacities were 1280 and 413 mA h g^{-1} at current densities of 0.5 and 10.0 A g^{-1}, respectively.	[S3]
Porous worm-like $NiMoO_4$ coaxially decorated electrospun carbon nanofiber	Hydrothermal method	The discharge capacities were 1132 and 503 mA h g^{-1} at current densities of 0.5 and 2.0 A g^{-1}, respectively.	[S4]
Hierarchical free-standing $NiMoO_4$/reduced graphene oxide membrane	Hydrothermal method & vacuum filtration	The discharge capacities were 1116 and 690 mA h g^{-1} at current densities of 0.25 and 4.0 A g^{-1}, respectively.	[S5]
Hierarchical $NiMoO_4$ nanowire	Hydrothermal method	The discharge capacities were 1338 and 231 mA h g^{-1} at current densities of 0.1 and 1.0 A g^{-1}, respectively.	[S6]
Phase-pure β-$NiMoO_4$ yolk-shell spheres	Spray pyrolysis	The discharge capacities were 1247 and 612 mA h g^{-1} at current densities of 0.5 and 5.0 A g^{-1}, respectively.	[S7]
Yolk-shell-structured microspheres composed of N-doped-carbon-coated $NiMoO_4$ hollow nanospheres	**Spray pyrolysis & Kirkendall diffusion**	**The discharge capacities were 1267 and 757 mA h g^{-1} at current densities of 0.5 and 10.0 A g^{-1}, respectively.**	**Our work**

References

[S1] K. Xiao, L. Xia, G. Liu, S. Wang, L.-X. Ding, and H. Wang, *J. Mater. Chem. A*, 2015, **3**, 6128-6135.

[S2] B. Wang, S. Li, X. Wu, W. Tian, J. Liu, and M. Yu, *J. Mater. Chem. A*, 2015, **3**, 13691-13698.

[S3] J.-S. Park, J. S. Cho, and Y. C. Kang, *J. Power Sources*, 2018, **379**, 278-287.

[S4] X. Tian, X. Li, T. Yang, K. Wang, H. Wang, Y. Song, Z. Liu, and Q. Guo, *Appl. Surf. Sci.*, 2018, **434**, 49-56.

[S5] X. Li, J. Bai, and H. Wang, *J. Solid State Electrochem.* 2018, **22**, 2659-2669.

[S6] J. Chen, R. Zhao, T. Wang, L. Li, and Q. Liu, *IOP Conf. Ser.: Mater. Sci. Eng.*, 2017, **274**, 012163.

[S7] J. H. Ahn, G. D. Park, Y. C. Kang, and J.-H. Lee, *Electrochim. Acta*, 2015, **174**, 102-110.